

# Effects of finite nucleon size, vacuum polarization, and electromagnetic spin-orbit interaction on nuclear binding energies and radii in spherical nuclei

Tomoya Naito (内藤智也),<sup>1,2</sup> Xavier Roca-Maza,<sup>3,4</sup> Gianluca Colò,<sup>3,4</sup> and Haozhao Liang (梁豪兆)<sup>2,1</sup>

<sup>1</sup>*Department of Physics, Graduate School of Science,  
The University of Tokyo, Tokyo 113-0033, Japan*

<sup>2</sup>*RIKEN Nishina Center, Wako 351-0198, Japan*

<sup>3</sup>*Dipartimento di Fisica, Università degli Studi di Milano, Via Celoria 16, 20133 Milano, Italy*

<sup>4</sup>*INFN, Sezione di Milano, Via Celoria 16, 20133 Milano, Italy*

(Dated: June 17, 2020)

The electromagnetic effects of the finite size of the nucleon are implemented self-consistently on top of the Skyrme Hartree-Fock calculation, where the electric form factors of both protons and neutrons are considered. Furthermore, the vacuum polarization and the electromagnetic spin-orbit interaction are taken into account. The self-consistent finite-size effects give a different Coulomb potential from the conventional one and affect the neutrons as well. The contribution of the finite-size effects to the total energy reaches 7 MeV in <sup>208</sup>Pb. The vacuum polarization and the electromagnetic spin-orbit interaction are also non-negligible, especially in the heavy nuclei. These effects provide a comparable contribution of the total energy to that of the isospin symmetry-breaking terms of the nuclear interaction. The mirror nuclei mass difference in <sup>48</sup>Ca–<sup>48</sup>Ni is also studied, and its value is improved by approximately one order of magnitude.

## I. INTRODUCTION

Atomic nuclei are quantum many-body systems composed of protons and neutrons, which interact with each other by the nuclear and Coulomb interactions. It is known that the nuclear interaction is much stronger than the Coulomb interaction, and thus the main contribution to the nuclear properties comes from the nuclear interaction. Nevertheless, the study of the Coulomb effects on the properties is also important, since the Coulomb interaction and the isospin symmetry-breaking (ISB) terms of the nuclear interaction are entangled to each other in some particular nuclear properties, such as the superallowed  $\beta$  decay [1, 2], the energy difference of the mirror nuclei and its Nolen-Schiffer anomaly [3–9], and the isobaric analog states (IASs) [10–12]. Recently, to study such ISB effects, a parametrization of the ISB terms of the nuclear interaction that can reproduce the mirror and triplet displacement energies on top of a Skyrme functional was proposed [13, 14]. From these and other works, it is evident that medium effects are relevant for those ISB terms, and the approximation of using the bare coupling constants is not adequate. Our current work does not address the important question of understanding the relationship between bare and effective ISB forces, but rather it focuses on a complementary and yet relevant issue: Our scope is to study the other Coulomb-related terms in DFT more precisely than has been done so far.

The density functional theory (DFT) [15, 16] is one of the powerful and widely used methods to solve the quantum many-body problem. In the DFT for nuclear physics, the ground-state energy is usually given by

$$E_{\text{gs}} = T_0 + E_{\text{nucl}}[\rho_p, \rho_n] + E_{\text{Cd}}[\rho_{\text{ch}}] + E_{\text{Cx}}[\rho_{\text{ch}}], \quad (1)$$

where  $T_0$  is the Kohn-Sham kinetic energy, and  $E_{\text{nucl}}$ ,  $E_{\text{Cd}}$ , and  $E_{\text{Cx}}$  are the energy density functionals (EDFs)

of nuclear, Coulomb direct, and Coulomb exchange parts, respectively. Here,  $\rho_p$  and  $\rho_n$  are the ground-state density distributions of protons and neutrons, respectively, and  $\rho_{\text{ch}}$  is the charge density distribution [17–19]. Since the nuclear EDF  $E_{\text{nucl}}$  is usually fit to the experimental data with certain Ansätze, such as the Skyrme type [20], the Gogny type [21], and the relativistic one [22, 23], because of the missing knowledge of the nuclear force in medium,  $E_{\text{nucl}}$  includes the Coulomb correlation as well as the nuclear one implicitly. In contrast, the Coulomb EDFs,  $E_{\text{Cd}}$  and  $E_{\text{Cx}}$ , are deduced theoretically as accurately as possible, since the Coulomb interaction is well known.

Although the Coulomb EDFs can be given fully theoretically, the Hartree-Fock-Slater [24, 25] or even Hartree approximation has been widely used [17, 18]. Recently, effects of the exact-Fock treatment [26–28] and those beyond the Hartree-Fock-Slater approximation, the so-called generalized gradient approximation (GGA) [29, 30], were discussed in the context of the nuclear DFT to achieve more accurate evaluation of the Coulomb contribution to the total energy.

Moreover, the role of the Coulomb functional has several open questions. For example, it was suggested that the Coulomb exchange term is almost canceled out by the ISB terms of the nuclear force, and thus the Skyrme functionals fit without the Coulomb exchange term reproduce the masses better than those with it [31, 32]. The effective charge in the nuclear DFT has also been discussed [33, 34]. Recently, Dong *et al.* [34] showed that, in the Hartree-Fock-Slater approximation, i.e., the local density approximation (LDA) for the Coulomb exchange term, introducing the effective coupling constant  $e_0^2 = e^2(1 + aZ^{-2/3})$  reproduces the isobaric multiplet mass equation well. They also discussed that this effective coupling constant includes all the possible electromagnetic (EM) contribution, such as the difference be-

tween the LDA and the exact-Fock, the finite-size effects, and the vacuum polarization.

The Coulomb EDFs  $E_{Cd}$  and  $E_{Cx}$  are, in principle, written in terms of the charge density  $\rho_{ch}$  [35], because the Coulomb interaction affects the charge itself instead of the point protons. Nevertheless, the protons and neutrons are assumed to be point particles, i.e.,  $\rho_{ch} \equiv \rho_p$  is assumed (hereafter, this approximation is called the point-particle approximation), in most of the self-consistent nuclear DFT. Only a few works, e.g., Refs. [12, 32, 36], considered the difference between  $\rho_{ch}$  and  $\rho_p$ .<sup>1</sup> It was shown that the finite-size effects of nucleons, i.e., the difference between  $\rho_{ch}$  and  $\rho_p$ , are non-negligible in the energy of the isobaric analog state  $E_{IAS}$  [12, 36]. Moreover, it was shown in Refs. [12, 36] that the vacuum polarization is also non-negligible in  $E_{IAS}$ .

Although these discussions related to the Coulomb interaction have been done for decades as mentioned above, deeper and self-consistent analysis is still desired. Thus, in this paper, the finite-size effects of nucleons are implemented to the self-consistent steps of the Skyrme Hartree-Fock calculation. The electric form factors of both protons and neutrons are considered. Also, other possible EM contributions, i.e., the vacuum polarization and the EM spin-orbit interaction, are considered.

This paper is organized as follows: First, the theoretical framework is given in Sec. II. Second, the simple estimation of systematic behavior of each effect is discussed in Sec. III. Then, the Skyrme Hartree-Fock calculation is performed to discuss systematics and to compare experimental data of mirror nuclei mass difference in Sec. IV. Finally, the conclusion and future perspectives are given in Sec. V.

## II. THEORETICAL FRAMEWORK

In this section, the theoretical frameworks of the finite-size effects, the vacuum polarization, and the EM spin-orbit interaction are shown. The Coulomb functional is accordingly composed of three terms: the Coulomb direct term  $E_{Cd}$ , the Coulomb exchange term  $E_{Cx}$ , and the vacuum polarization term  $E_{VP}$ . Equation (1) is now modified as

$$E_{gs} = T_0 + E_{nucl}[\rho_p, \rho_n] + E_{Cd}[\rho_{ch}] + E_{Cx}[\rho_{ch}] + E_{VP}[\rho_{ch}], \quad (2)$$

and correspondingly the effective potential is

$$V_{eff\tau}(\mathbf{r}) = V_{nucl\tau}(\mathbf{r}) + V_{Cd\tau}(\mathbf{r}) + V_{Cx\tau}(\mathbf{r}) + V_{VP\tau}(\mathbf{r}), \quad (3)$$

where  $\tau = p$  ( $n$ ) for protons (neutrons), and  $V_{nucl\tau}$ ,  $V_{Cd\tau}$ ,  $V_{Cx\tau}$ , and  $V_{VP\tau}$  are the effective potentials coming from

the nuclear force, Coulomb direct and exchange terms, and the vacuum polarization, respectively.

In  $E_{Cd}$  and  $E_{Cx}$ , the finite-size effects of nucleons are considered, where the Coulomb direct term  $E_{Cd}$  holds the conventional form

$$E_{Cd}[\rho_{ch}] = \frac{e^2}{2} \iint \frac{\rho_{ch}(\mathbf{r}) \rho_{ch}(\mathbf{r}')}{|\mathbf{r} - \mathbf{r}'|} d\mathbf{r} d\mathbf{r}'. \quad (4)$$

The EM spin-orbit interaction is considered perturbatively.

### A. Coulomb Exchange Functional in Generalized Gradient Approximation

In principle, the nonlocal form of the Fock term

$$E_F = -\frac{e^2}{2} \sum_{i,j} \iint \frac{\psi_i^*(\mathbf{r}) \psi_j^*(\mathbf{r}') \psi_i(\mathbf{r}') \psi_j(\mathbf{r})}{|\mathbf{r} - \mathbf{r}'|} d\mathbf{r} d\mathbf{r}' \quad (5)$$

should be used for the Coulomb exchange term in the point-particle approximation, where  $\psi_i$  is the single-particle wave function of protons. The GGA for the Coulomb exchange term was proposed in the context of the nuclear DFT [29, 30]. The GGA functional reproduces the Coulomb exact-Fock energy within 100 keV error. In this paper, the GGA Coulomb exchange functional is used instead of the exact-Fock term, because writing the functional in terms of density has the advantage of considering the finite-size effects, which we discuss later.

The GGA Coulomb exchange functional is written as [37]

$$E_{Cx}[\rho_{ch}] = \int \varepsilon_{Cx}^{LDA}(\rho_{ch}(\mathbf{r})) F(s(\mathbf{r})) \rho_{ch}(\mathbf{r}) d\mathbf{r}, \quad (6)$$

where  $\varepsilon_{Cx}^{LDA}$  is the LDA exchange energy density

$$\varepsilon_{Cx}^{LDA}(\rho_{ch}) = -\frac{3e^2}{4} \left(\frac{3}{\pi}\right)^{1/3} \rho_{ch}^{1/3}, \quad (7)$$

$s$  is the dimensionless density gradient

$$s = \frac{|\nabla\rho_{ch}|}{2k_F\rho_{ch}}, \quad k_F = (3\pi^2\rho_{ch})^{1/3}, \quad (8)$$

and  $F$  is the GGA enhancement factor. Here, the modified Perdew-Burke-Ernzerhof GGA enhancement factor

$$F(s) = 1 + \kappa - \frac{\kappa}{1 + \lambda\mu s^2/\kappa}, \quad (9)$$

$$\mu = 0.21951, \quad \kappa = 0.804, \quad (10)$$

with  $\lambda = 1.25$  [30] is used.

<sup>1</sup> Note that the nuclear interaction is constructed as the nucleons are point particles, and thus the finite-size effects need not be considered in  $E_{nucl}$ .

## B. Finite-size effects of nucleons

In most works, protons and neutrons are assumed to be point particles, and thus  $\rho_{\text{ch}} \equiv \rho_p$  is assumed in the self-consistent steps and the calculation of  $E_{\text{gs}}$ . The difference between  $\rho_{\text{ch}}$  and  $\rho_p$  is considered explicitly in the self-consistent steps in this paper. Only the electric form factors of nucleons are considered, while the magnetic form factors are not considered in the single-particle wave functions since they appear in higher ( $1/c^2$ ) and require us to consider the EM spin-orbit interaction self-consistently. Instead, effects of the magnetic form factors are considered in the single-particle energy via the EM

spin-orbit interaction, as discussed later.

### 1. Electric form factor

The charge density distribution  $\rho_{\text{ch}}$  is written in terms of the electric form factors of protons and neutrons,  $\tilde{G}_{\text{Ep}}$  and  $\tilde{G}_{\text{En}}$ , and the density distributions of protons and neutrons,  $\rho_p$  and  $\rho_n$  [38],

$$\tilde{\rho}_{\text{ch}}(q) = \tilde{G}_{\text{Ep}}(q^2) \tilde{\rho}_p(q) + \tilde{G}_{\text{En}}(q^2) \tilde{\rho}_n(q), \quad (11)$$

where the quantities with tilde denote those in the momentum space. For example,  $\tilde{\rho}_p$  reads

$$\tilde{\rho}_p(q) = \frac{1}{(2\pi)^{3/2}} \int \rho_p(r) e^{-i\mathbf{q}\cdot\mathbf{r}} d\mathbf{r} = \sqrt{\frac{2}{\pi}} \int_0^\infty \rho_p(r) \frac{\sin(qr)}{qr} r^2 dr, \quad (12)$$

with the Fourier transformation of  $\rho_p$ . Here, the spherical symmetry is assumed for  $\rho_p$ ,  $\rho_n$ , and  $\rho_{\text{ch}}$ .

The electric form factors  $\tilde{G}_{\text{Ep}}$  and  $\tilde{G}_{\text{En}}$  are measured by the electron scattering of protons and neutrons, and their forms are taken from Ref. [39] as

$$\tilde{G}_{\text{E}\tau}(q^2) = \frac{a_{10\tau}}{(1+q^2/a_{11\tau})^2} + \frac{a_{20\tau}}{(1+q^2/a_{21\tau})^2} + a_{b\tau} q^2 \left[ \exp\left\{-\frac{1}{2}\left(\frac{q-q_{b\tau}}{\sigma_{b\tau}}\right)^2\right\} + \exp\left\{-\frac{1}{2}\left(\frac{q+q_{b\tau}}{\sigma_{b\tau}}\right)^2\right\} \right], \quad (13)$$

where the corresponding parameters are listed in Table I.

In this paper,  $\rho_{\text{ch}}$  given in Eq. (11) is used in both the self-consistent steps and the calculation of  $E_{\text{gs}}$ , instead of the point-particle approximation. Precisely,  $\rho_p$  and  $\rho_n$  are calculated from the single-particle wave functions  $\psi_i$ , and  $\rho_{\text{ch}}$  is calculated from Eq. (11) in each self-consistent step. The effective potential  $V_{\text{eff}\tau}$  for  $\psi_i$  is derived from  $\rho_{\text{ch}}$  as well as  $\rho_p$  and  $\rho_n$ . As a result, the Coulomb potential in  $V_{\text{eff}\tau}$  is different from that calculated in the point-particle approximation. Details are shown as follows.

### 2. Effective potential with finite-size effects

The effective potential of the nucleon  $\tau$  is, in general, defined as [20, 40]

$$V_{\text{eff}\tau}(\mathbf{r}) = \frac{\delta E[\rho_p, \rho_n]}{\delta \rho_\tau(\mathbf{r})}. \quad (14)$$

Once the finite-size effects are considered, i.e.,  $\rho_{\text{ch}} \neq \rho_p$ , the chain rule of the functional derivative [40]

$$\frac{\delta}{\delta f(\mathbf{r})} = \int \frac{\delta g(\mathbf{r}')}{\delta f(\mathbf{r})} \frac{\delta}{\delta g(\mathbf{r}')} d\mathbf{r}' \quad (15)$$

should be applied to the Coulomb terms  $E_{\text{Cd}}$  and  $E_{\text{Cx}}$ .

The charge density distribution in the real space is

$$\rho_{\text{ch}}(r) = \frac{1}{(2\pi)^{3/2}} \left[ \int G_{\text{Ep}}(|\mathbf{r}-\mathbf{r}'|) \rho_p(r') d\mathbf{r}' + \int G_{\text{En}}(|\mathbf{r}-\mathbf{r}'|) \rho_n(r') d\mathbf{r}' \right], \quad (16)$$

where  $G_{\text{E}\tau}$  are the electric form factors of the nucleons

in the real space defined as

$$G_{\text{E}\tau}(r) = \sqrt{\frac{2}{\pi}} \int_0^\infty \tilde{G}_{\text{E}\tau}(q^2) \frac{\sin(qr)}{qr} q^2 dq, \quad (17)$$

TABLE I. Parameters of the electric form factors  $\tilde{G}_{Ep}$  and  $\tilde{G}_{En}$  taken from Ref. [39]. Uncertainty is not shown in this table.

$\tau$	$a_{10\tau}$	$a_{11\tau}$ (GeV <sup>2</sup> /c <sup>2</sup> )	$a_{20\tau}$	$a_{21\tau}$ (GeV <sup>2</sup> /c <sup>2</sup> )	$a_{b\tau}$ (c <sup>2</sup> /GeV <sup>2</sup> )	$q_{b\tau}$ (GeV/c)	$\sigma_{b\tau}$ (GeV/c)
Proton	1.041	0.765	-0.041	6.2	-0.23	0.07	0.27
Neutron	1.04	1.73	-1.04	1.54	0.23	0.29	0.20

since the product in the momentum space is identical to the convolution in the real space as

$$\tilde{f}(q) \tilde{g}(q) = \sqrt{\frac{2}{\pi}} \int_0^\infty \left[ \frac{1}{(2\pi)^{3/2}} (f * g)(r) \right] \frac{\sin(qr)}{qr} r^2 dr, \quad (18)$$

$$(f * g)(r) = \int f(|\mathbf{r} - \mathbf{r}'|) g(r') d\mathbf{r}'. \quad (19)$$

From Eqs. (15) and (16), the functional derivative with respect to  $\rho_{\text{ch}}$  reads

$$\begin{aligned} \frac{\delta}{\delta\rho_\tau(r)} &= \int \frac{\delta\rho_{\text{ch}}(r')}{\delta\rho_\tau(r)} \frac{\delta}{\delta\rho_{\text{ch}}(r')} d\mathbf{r}' \\ &= \frac{1}{(2\pi)^{3/2}} \int G_{E\tau}(|\mathbf{r} - \mathbf{r}'|) \frac{\delta}{\delta\rho_{\text{ch}}(r')} d\mathbf{r}'. \end{aligned} \quad (20)$$

Combining Eqs. (14) and (20), the Coulomb potential for nucleons with the finite-size effects reads

$$\begin{aligned} V_{C\tau}(r) &= \frac{\delta E_C[\rho_{\text{ch}}]}{\delta\rho_\tau(r)} \\ &= \int \frac{\delta E_C[\rho_{\text{ch}}]}{\delta\rho_{\text{ch}}(r')} \frac{\delta\rho_{\text{ch}}(r')}{\delta\rho_\tau(r)} d\mathbf{r}' \\ &= \frac{1}{(2\pi)^{3/2}} \int \mathcal{V}_C[\rho_{\text{ch}}](r') G_{E\tau}(|\mathbf{r} - \mathbf{r}'|) d\mathbf{r}', \end{aligned} \quad (21)$$

where  $E_C[\rho_{\text{ch}}] = E_{\text{Cd}}[\rho_{\text{ch}}] + E_{\text{Cx}}[\rho_{\text{ch}}]$ , and  $\mathcal{V}_C$  is the conventional form of the Coulomb potential, but expressing in terms of  $\rho_{\text{ch}}$  instead, e.g.,

$$\begin{aligned} \mathcal{V}_C[\rho_{\text{ch}}](\mathbf{r}) &= \mathcal{V}_{\text{Cd}}[\rho_{\text{ch}}](\mathbf{r}) + \mathcal{V}_{\text{Cx}}[\rho_{\text{ch}}](\mathbf{r}) \\ &= e^2 \int \frac{\rho_{\text{ch}}(\mathbf{r}')}{|\mathbf{r} - \mathbf{r}'|} d\mathbf{r}' - e^2 \left(\frac{3}{\pi}\right)^{1/3} [\rho_{\text{ch}}(\mathbf{r})]^{1/3} \end{aligned} \quad (22)$$

in the LDA form. For the GGA form, see Ref. [30]. It should be noted that the Coulomb potential in the momentum space is

$$\tilde{V}_{C\tau}[\rho_{\text{ch}}](q) = \tilde{\mathcal{V}}_C[\rho_{\text{ch}}](q) \tilde{G}_{E\tau}(q^2). \quad (23)$$

Let us compare the Coulomb potential with the finite-size effects proposed in this paper and that used in previous works such as Refs. [12, 32, 41]. The Coulomb potential without the finite-size effects corresponds to  $\mathcal{V}_C$

calculated with  $\rho_p$ , i.e.,  $\mathcal{V}_C[\rho_p]$ . The Coulomb potential with the finite-size effects in previous works [12, 32, 41] is calculated with  $\rho_{\text{ch}}$  when the potential is calculated, i.e.,  $\mathcal{V}_C[\rho_{\text{ch}}]$ . This corresponds to  $\tilde{G}_{Ep} \equiv 1$  and  $\tilde{G}_{En} \equiv 0$  being used in Eq. (23), in which case the self-consistency shown in Eqs. (14) and (20) is no longer valid. In contrast, the Coulomb potential with the finite-size effects in this work is derived self-consistently. Hereafter, the finite-size effects in the previous works are simply called ‘‘conventional finite-size effects,’’ and those in this work are ‘‘self-consistent finite-size effects.’’ It should be emphasized that the Coulomb potential for the neutrons,  $\mathcal{V}_{Cn}$ , does not vanish within the self-consistent finite-size effects since  $G_{En} \neq 0$ , whereas the conventional Coulomb potential  $\mathcal{V}_C$  affects only protons.

### C. Vacuum polarization

The vacuum polarization is the lowest-order correction of quantum electrodynamics (QED) for the Coulomb interaction [42]. The effective one-body potential of the vacuum polarization for a charged particle  $-e$  under the Coulomb potential caused by the charge distribution  $\rho_{\text{ch}}$  is known as the Uehling potential [43]. In the case of atomic nuclei, the charge of protons is  $+e$ , and thus the sign of the potential is opposite to the original Uehling potential as

$$V_{\text{VP}}(\mathbf{r}) = \frac{2}{3} \frac{\alpha e^2}{\pi} \int \frac{\rho_{\text{ch}}(\mathbf{r}')}{|\mathbf{r} - \mathbf{r}'|} \mathcal{K}_1\left(\frac{2}{\lambda_e} |\mathbf{r} - \mathbf{r}'|\right) d\mathbf{r}', \quad (24)$$

where

$$\mathcal{K}_1(x) = \int_1^\infty e^{-xt} \left(\frac{1}{t^2} + \frac{1}{2t^4}\right) \sqrt{t^2 - 1} dt, \quad (25)$$

$\alpha$  is the fine-structure constant, and  $\lambda_e = 386.15926796$  fm is the reduced Compton wavelength of electrons<sup>2</sup> [44]. Correspondingly, the EDF for the vacuum polarization is written as

$$E_{\text{VP}}[\rho_{\text{ch}}] = \frac{1}{2} \int \rho_{\text{ch}}(\mathbf{r}) V_{\text{VP}}(\mathbf{r}) d\mathbf{r}. \quad (26)$$

Once spherical symmetry is assumed, Eq. (24) is written as [45]

$$V_{\text{VP}}(r) = \frac{2\alpha e^2 \tilde{\lambda}_e}{3r} \int_0^\infty \left[ \mathcal{K}_0 \left( \frac{2}{\tilde{\lambda}_e} |r - r'| \right) - \mathcal{K}_0 \left( \frac{2}{\tilde{\lambda}_e} |r + r'| \right) \right] \rho_{\text{ch}}(r') r' dr', \quad (27)$$

where

$$\begin{aligned} \mathcal{K}_0(x) &= - \int_{-\infty}^x \mathcal{K}_1(x') dx' \\ &= \int_1^\infty e^{-xt} \left( \frac{1}{t^3} + \frac{1}{2t^5} \right) \sqrt{t^2 - 1} dt. \end{aligned} \quad (28)$$

In this work, this potential is assumed to affect only protons. According to the treatment of the finite-size effects in the DFT scheme discussed in Sec. II B, the vacuum polarization potential for protons and neutrons,  $V_{\text{VP}\tau}$ , are  $\delta E_{\text{VP}}/\delta\rho_\tau$ , slightly different from the original  $V_{\text{VP}}$ . However, this difference must be tiny. Therefore,  $V_{\text{VP}}$  is applied to protons, and the vacuum polarization potential for neutrons is neglected, while  $\rho_{\text{ch}}$  is used for calculating  $V_{\text{VP}}$  in Eq. (27). This corresponds to the conventional treatment of the finite-size effects in the

Coulomb potential.

#### D. Electromagnetic spin-orbit interaction

The protons and neutrons move inside the charge distribution  $\rho_{\text{ch}}$ . On the frame of a nucleon, this charge distribution is regarded as moving and the moving charge distribution generates a magnetic field, which interacts with the spin of the nucleon. This interaction is the spin-orbit interaction.

In this work, the EM spin-orbit interaction is considered by using the first-order perturbation theory. The effects on the single-particle orbitals and potentials are neglected since this interaction affects the single-particle energies by less than 100 keV. The correction due to the EM spin-orbit interaction for the single-particle energy is [46]

$$\begin{aligned} \Delta\varepsilon_i &= \frac{\hbar^2 c^2}{2m^2 c^4} x_i \langle \hat{l}_i \cdot \hat{s}_i \rangle \int_0^\infty \frac{[u_i(r)]^2}{r} \frac{d\mathcal{V}_C(r)}{dr} dr \\ &= \frac{\hbar^2 c^2}{2m^2 c^4} x_i \left[ j_i(j_i + 1) - l_i(l_i + 1) - \frac{3}{4} \right] \int_0^\infty \frac{[u_i(r)]^2}{r} \frac{d\mathcal{V}_C(r)}{dr} dr, \end{aligned} \quad (29)$$

where  $\hat{l}_i$  and  $\hat{s}_i$  are its orbital and spin angular-momentum operators,  $ru_i(r)$  is the radial part of single-particle wave function, and  $l_i$  and  $j_i$  are the azimuthal quantum number and total angular momentum, respectively. The quantity  $x_i$  is related to the  $g$  factors as [44]

$$x_i = \begin{cases} g_p - 1 = 4.5856946893 & \text{for protons,} \\ g_n = -3.82608545 & \text{for neutrons.} \end{cases} \quad (30)$$

This equation is the same as the spin-orbit interaction for hydrogen-like atoms [47], while the  $g$  factors of nucleons are used instead. Here, 1 in Eq. (30) corresponds to the charge of protons. In this calculation, the Coulomb potential without the finite-size effects  $\mathcal{V}_C[\rho_p]$  is used, since the correction itself is expected to be small, and thus it does not need to take into account the finite-size correction in  $\mathcal{V}_C[\rho_{\text{ch}}]$ .

### III. SIMPLE ESTIMATION OF SYSTEMATIC BEHAVIORS

Before the numerical calculation, simple estimations are performed in this section to understand the systematic behavior of the contributions of the finite-size effects and the vacuum polarization to the total energy. The hard-sphere distribution is assumed for protons:

$$\rho_p(r) = \begin{cases} \rho_0^p & r < R_p, \\ 0 & r > R_p, \end{cases} \quad (31)$$

where  $R_p$  is the radius of the proton distribution and

$$\rho_0^p = \frac{3Z}{4\pi R_p^3} \quad (32)$$

is held. The saturation density of protons,

$$\rho_0^p = \frac{1}{2}\rho_0 \simeq 0.08 \text{ fm}^{-3}, \quad (33)$$

together with

$$R_p = \left( \frac{3Z}{4\pi\rho_0^p} \right)^{1/3}, \quad (34)$$

<sup>2</sup> The dominant contribution of a virtual particle-antiparticle pair produced in a photon propagator is the lightest fermions, i.e., electrons. Therefore, quantities appeared in the Uehling potential are still those for electrons even though the potential is applied to protons.

are used for estimation of coefficients, where  $\rho_0$  is the saturation density of atomic nuclei. Accordingly, the neutron and charge distributions are also assumed to be hard spheres. When the finite-size effects are considered, we use proton and neutron radii,  $\langle r_p^2 \rangle$  and  $\langle r_n^2 \rangle$ , consistent with the form factors (17). Note that smaller or larger values of proton radius that are recently debated in the literature do not affect our simple estimation significantly.

At first, the estimation under the point-particle approximation is discussed. The Coulomb direct potential is

$$\begin{aligned} V_{\text{Cd}}^{\text{point}}(r) &= e^2 \int \frac{\rho_p(r')}{|\mathbf{r} - \mathbf{r}'|} d\mathbf{r}' \\ &= \begin{cases} \frac{Ze^2}{2R_p} \left(3 - \frac{r^2}{R_p^2}\right) & r < R_p, \\ \frac{Ze^2}{r} & r > R_p, \end{cases} \end{aligned} \quad (35)$$

and thus the Coulomb direct energy is

$$\begin{aligned} E_{\text{Cd}}^{\text{point}} &= \frac{1}{2} \int \rho_p(r) V_{\text{Cd}}^{\text{point}}(r) dr \\ &= \frac{3e^2 Z^2}{5 R_p} \\ &= \frac{3e^2}{5} \left(\frac{4\pi\rho_0^p}{3}\right)^{1/3} Z^{5/3} \\ &\simeq 0.60Z^{5/3} \text{ MeV}. \end{aligned} \quad (36)$$

The Coulomb exchange energy is

$$\begin{aligned} E_{\text{Cx}}^{\text{point}} &= -\frac{3e^2}{4} \left(\frac{3}{\pi}\right)^{1/3} \int [\rho_p(r)]^{4/3} dr \\ &= -\frac{3e^2}{4} \left(\frac{9}{4\pi^2}\right)^{1/3} \frac{Z^{4/3}}{R_p} \\ &= -\frac{3e^2}{4} \left(\frac{3\rho_0^p}{\pi}\right)^{1/3} Z \\ &\simeq -0.46Z \text{ MeV}. \end{aligned} \quad (37)$$

Let us consider the finite-size effects for the Coulomb energy. Hereafter, the superscripts associated with energies describe which finite-size effects are considered; “point,” “ $p$ -finite,” and “ $pn$ -finite” mean the energies calculated with the point-particle approximation, the proton finite-size effect, and both the proton and the neutron finite-size effects, respectively. Only the finite-size correction to the Coulomb direct energy is discussed here, since the finite-size effects should be a small correction and the main contribution of the Coulomb energy to the total energy is the direct term. The relationship between

the radii is assumed to be [48]

$$R_{\text{ch}}^2 \simeq R_p^2 + \langle r_p^2 \rangle + \frac{N}{Z} \langle r_n^2 \rangle, \quad (38)$$

where  $R_{\text{ch}}$  is the charge radius of the nucleus. Here, the contribution of the EM spin-orbit interaction is not considered in Eq. (38). The Coulomb direct energy with the finite-size effects is the same as Eq. (36), while  $R_{\text{ch}}$  is used instead of  $R_p$ , i.e.,

$$E_{\text{Cd}}^{\text{finite}} = \frac{3e^2 Z^2}{5 R_{\text{ch}}}. \quad (39)$$

The contribution of the proton finite-size effect for the total energy is estimated with  $\langle r_n^2 \rangle = 0$  in  $R_{\text{ch}}$  of Eq. (38) as

$$\begin{aligned} E_C^{p\text{-finite}} - E_C^{\text{point}} &\simeq E_{\text{Cd}}^{p\text{-finite}} - E_{\text{Cd}}^{\text{point}} \\ &= \frac{3e^2}{5} Z^2 \left( \frac{1}{R_{\text{ch}}^{p\text{-finite}}} - \frac{1}{R_p} \right) \\ &= \frac{3e^2}{5} Z^2 \left[ \frac{1}{\sqrt{R_p^2 + \langle r_p^2 \rangle}} - \frac{1}{R_p} \right] \\ &\simeq -\frac{3e^2 \langle r_p^2 \rangle Z^2}{10 R_p^3} \\ &= -\frac{2\pi e^2 \rho_0^p \langle r_p^2 \rangle}{5} Z \\ &\simeq -0.11Z \text{ MeV}. \end{aligned} \quad (40)$$

The contribution of the neutron finite-size effect to the total energy is

$$\begin{aligned} E_C^{pn\text{-finite}} - E_C^{p\text{-finite}} &\simeq E_{\text{Cd}}^{pn\text{-finite}} - E_{\text{Cd}}^{p\text{-finite}} \\ &= \frac{3e^2}{5} Z^2 \left( \frac{1}{R_{\text{ch}}^{pn\text{-finite}}} - \frac{1}{R_{\text{ch}}^{p\text{-finite}}} \right) \\ &= \frac{3e^2}{5} Z^2 \left[ \frac{1}{\sqrt{R_p^2 + \langle r_p^2 \rangle + \frac{N}{Z} \langle r_n^2 \rangle}} - \frac{1}{\sqrt{R_p^2 + \langle r_p^2 \rangle}} \right] \\ &\simeq -\frac{3e^2 \langle r_n^2 \rangle}{10} \frac{NZ}{(R_p^2 + \langle r_p^2 \rangle)^{3/2}} \\ &\simeq -\frac{3e^2 \langle r_n^2 \rangle NZ}{10 R_p^3} \\ &= -\frac{2\pi e^2 \rho_0^p \langle r_n^2 \rangle}{5} N \\ &\simeq 0.010N \text{ MeV}. \end{aligned} \quad (41)$$

Since  $\langle r_p^2 \rangle > 0$  and  $\langle r_n^2 \rangle < 0$ , the coefficient in Eq. (41) is positive, whereas that in Eq. (40) is negative.

At the end of this section, the energy of the vacuum polarization is estimated. It reads

$$\begin{aligned}
E_{\text{VP}} &= \frac{1}{2} \int \rho_{\text{ch}}(r) V_{\text{VP}}(r) dr \\
&\simeq 2\pi \int_0^\infty \rho_p(r) V_{\text{VP}}(r) r^2 dr \\
&= 2\pi \rho_0^p \int_0^{R_p} V_{\text{VP}}(r) r^2 dr \\
&= 2\pi \rho_0^p \frac{2\alpha e^2 \lambda_e}{3} \int_0^{R_p} \int_0^\infty \left[ \mathcal{K}_0\left(\frac{2}{\lambda_e} |r-r'|\right) - \mathcal{K}_0\left(\frac{2}{\lambda_e} |r+r'|\right) \right] \rho_{\text{ch}}(r') r' dr' r dr \\
&\simeq 2\pi (\rho_0^p)^2 \frac{2\alpha e^2 \lambda_e}{3} \int_0^{R_p} \int_0^{R_p} \left[ \mathcal{K}_0\left(\frac{2}{\lambda_e} |r-r'|\right) - \mathcal{K}_0\left(\frac{2}{\lambda_e} |r+r'|\right) \right] r' dr' r dr.
\end{aligned} \tag{42}$$

The first term of the integral in Eq. (42) is estimated as

$$\begin{aligned}
&\int_0^{R_p} \int_0^{R_p} \mathcal{K}_0\left(\frac{2}{\lambda_e} |r-r'|\right) r' dr' r dr \\
&= \int_0^{R_p} \int_0^{R_p} \int_1^\infty e^{-2c|r-r'|} \left(\frac{1}{t^3} + \frac{1}{2t^5}\right) \sqrt{t^2-1} dt r' dr' r dr \\
&= \int_1^\infty \int_0^{R_p} \left[ \int_0^r e^{-2c(r-r')} r' dr' + \int_r^{R_p} e^{2c(r-r')} r' dr' \right] r dr \left(\frac{1}{t^3} + \frac{1}{2t^5}\right) \sqrt{t^2-1} dt \\
&= \int_1^\infty \int_0^{R_p} \frac{r}{4c^2} \left[ 4cr + e^{-2cr} - e^{2c(r-R_p)} (1+2cR_p) \right] dr \left(\frac{1}{t^3} + \frac{1}{2t^5}\right) \sqrt{t^2-1} dt \\
&= \int_1^\infty \frac{3 - 6c^2 R_p^2 + 8c^3 R_p^3 - 3e^{-2cR_p} (1+2cR_p)}{24c^4} \left(\frac{1}{t^3} + \frac{1}{2t^5}\right) \sqrt{t^2-1} dt,
\end{aligned} \tag{43}$$

and the second term is

$$\begin{aligned}
\int_0^{R_p} \int_0^{R_p} \mathcal{K}_0\left(\frac{2}{\lambda_e} |r+r'|\right) r' dr' r dr &= \int_0^{R_p} \int_0^{R_p} \int_1^\infty e^{-2c|r+r'|} \left(\frac{1}{t^3} + \frac{1}{2t^5}\right) \sqrt{t^2-1} dt r' dr' r dr \\
&= \int_1^\infty \int_0^{R_p} \int_0^{R_p} e^{-2c(r+r')} r' dr' r dr \left(\frac{1}{t^3} + \frac{1}{2t^5}\right) \sqrt{t^2-1} dt \\
&= \int_1^\infty \frac{e^{-4cR_p} (1 - e^{2cR_p} + 2cR_p)^2}{16c^4} \left(\frac{1}{t^3} + \frac{1}{2t^5}\right) \sqrt{t^2-1} dt,
\end{aligned} \tag{44}$$

where  $c = t/\lambda_e$ . Combining Eqs. (42)–(44), we get

$$\begin{aligned}
&\int_0^{R_p} \int_0^{R_p} \left[ \mathcal{K}_0\left(\frac{2}{\lambda_e} |r-r'|\right) - \mathcal{K}_0\left(\frac{2}{\lambda_e} |r+r'|\right) \right] r' dr' r dr \\
&= \int_1^\infty \left[ \frac{3 - 6c^2 R_p^2 + 8c^3 R_p^3 - 3e^{-2cR_p} (1+2cR_p)}{24c^4} - \frac{e^{-4cR_p} (1 - e^{2cR_p} + 2cR_p)^2}{16c^4} \right] \left(\frac{1}{t^3} + \frac{1}{2t^5}\right) \sqrt{t^2-1} dt \\
&\simeq 0.0070 R_p^5 \text{ MeV}.
\end{aligned} \tag{45}$$

Finally, we can estimate Eq. (42) as

$$\begin{aligned}
E_{\text{VP}} &\simeq 2\pi (\rho_0^p)^2 \frac{2\alpha e^2 \lambda_e}{3} \times 0.0070 R_p^5 \text{ MeV} \\
&\simeq 0.0047 Z^{5/3} \text{ MeV}.
\end{aligned} \tag{46}$$

At the end of this section, effects of these terms on

the Coulomb displacement energy are discussed. The displacement energy is defined as [36]

$$E_{\text{dis}} = \frac{\langle \text{P} | T_+ [H, T_-] | \text{P} \rangle}{N}, \tag{47}$$

where  $|\text{P}\rangle$  is the parent nucleus,  $H$  is the total Hamiltonian, and  $T_\pm$  are the isospin raising and lowering opera-

tors. Auerbach *et al.* [36] estimated the contributions of the Coulomb exchange, proton finite-size effect, and the vacuum polarization as  $-900Z/A$  keV,  $\sim -100$  keV, and  $8.5Z/A^{1/3}$  keV, respectively.

Each contribution of the Coulomb energy to the displacement energy is calculated from the simple estimations as  $E_{C_i}^D - E_{C_i}^P$ , where  $E_{C_i}^P$  and  $E_{C_i}^D$  refer to the energies of each contribution for the parent and daughter nuclei, respectively. Since the proton and neutron numbers  $Z$  and  $N$  change to  $Z + 1$  and  $N - 1$  in the isobaric analog resonance, the contributions to the displacement energy of the Coulomb exchange, proton finite-size effect, neutron finite-size effect, and the vacuum polarization read approximately  $-460$  keV,  $-110$  keV,  $-10$  keV, and  $7.8Z^{2/3}$  keV, respectively. These values are consistent with Auerbach's estimation if  $Z \simeq A/2$  is assumed.

#### IV. THEORETICAL CALCULATION AND DISCUSSION

The finite-size effects, the vacuum polarization, and the EM spin-orbit interaction are implemented to the self-consistent Skyrme Hartree-Fock plus RPA code named SKYRME\_RPA [49]. The ISB terms of the nuclear force are also implemented to compare the contributions of the EM interaction with that of the ISB terms of nuclear force. Details of the ISB terms of nuclear force are shown in the appendix. In this calculation, spherical symmetry is assumed, and the pairing correlations are not considered. A box of 15 fm with 0.1 fm mesh is used. In each self-consistent step, the charge density distribution and the Coulomb potential are calculated with Eqs. (11) and (23), respectively, instead of the convolution in the real space. More precisely, in each self-consistent step, the nucleon densities  $\rho_\tau$  and the Coulomb potential  $\mathcal{V}_C$ , obtained by the SKYRME\_RPA code in the real space, are transformed to the momentum space, and then  $\tilde{\rho}_{\text{ch}}$  and  $\tilde{V}_C$  are derived and transformed back to the real space.

In this paper, the SAMi functional [50] is used for the nuclear EDF for most calculations, and the SAMi-ISB functional [12] is used instead when the isospin symmetry breaking originated from the nuclear interaction is considered explicitly.

One may wonder whether the Skyrme functional should be refitted. The coefficients of the Skyrme functionals are determined to reproduce the experimental total binding energies and density distributions of the selected nuclei. In this paper, our main motivation is to see how these corrections affect the nuclear properties in the Skyrme Hartree-Fock calculations instead of the comparison between the calculations and experimental data. In short, this is a sensitivity study. If we wished to compare with experimental data in detail, we would need a refit of the Skyrme functional.

#### A. Systematic calculation

First of all, the systematic behavior of the contributions of the finite-size effects, vacuum polarization, and EM spin-orbit interaction are discussed. Some doubly magic and semimagic nuclei are selected. The calculations are performed under the assumption of spherical symmetry without pairing, which is assumed not to affect the main conclusions of the present paper, even for the semi-magic nuclei.

In Table II, the total energies of the selected nuclei are shown, where contributions are considered step by step to see the effects of each term. In Fig. 1, the ratios of the Coulomb direct and exchange energies calculated with the finite-size effects to those without the finite-size effects,  $E_{C_i}^{\text{finite}}/E_{C_i}^{\text{point}}$  ( $i = d, x$ ), are shown as functions of the mass number  $A$ .

It is seen that the proton finite-size effect makes the nuclei more bound, for example, 580 keV and 8.2 MeV for  $^{16}\text{O}$  and  $^{208}\text{Pb}$ , respectively. In contrast, the neutron finite-size effect makes the nuclei less bound, for instance, 64 keV and 1.2 MeV for  $^{16}\text{O}$  and  $^{208}\text{Pb}$ , respectively.

From the point of view of the interaction, the finite-size effect of protons makes the Coulomb interaction effectively weaker, because  $\rho_{\text{ch}}$  distributes more extensive and dilute than  $\rho_p$  due to the proton finite size as shown in Eq. (38). In contrast, the finite-size effect of neutrons makes the Coulomb interaction effectively stronger, because the neutron radius  $\langle r_n^2 \rangle$  is negative and hence neutrons effectively behave as negative charge rather than as positive charge, which make  $\rho_{\text{ch}}$  distributes more compact and denser. The absolute value of the proton radius  $|\langle r_p^2 \rangle|$  is larger than that of the neutron radius  $|\langle r_n^2 \rangle|$ , and therefore, the proton finite-size effect is more significant than the neutron finite-size effect as shown in Fig. 1. Although the finite-size effects for light nuclei are more significant than those for the heavy nuclei since  $R_p$  is smaller, the absolute values themselves for the heavy nuclei are more significant. It should be noted that even though the neutron finite-size effect is smaller than the proton one, it is not small enough to be neglected in heavy nuclei.

As shown in Table II, the vacuum polarization makes the nuclei less bound, for example, 88 keV and 3.7 MeV for  $^{16}\text{O}$  and  $^{208}\text{Pb}$ , respectively. The vacuum polarization contributes to the total energy more than the difference between the exact-Fock and the LDA Coulomb exchange energies and the neutron finite-size effect. Hence, it is not small at all to be neglected in heavy nuclei.

Among the contributions of the finite-size effects and the vacuum polarization to the total energy, the proton finite-size effect is the dominant. The contribution of the vacuum polarization is larger than that of the neutron finite-size effect in the heavy nuclei, whereas they are comparable in the light nuclei.

Next, the systematic behaviors of these contributions to the total energy are discussed. For this estimation, the Coulomb direct and exchange energies calculated with



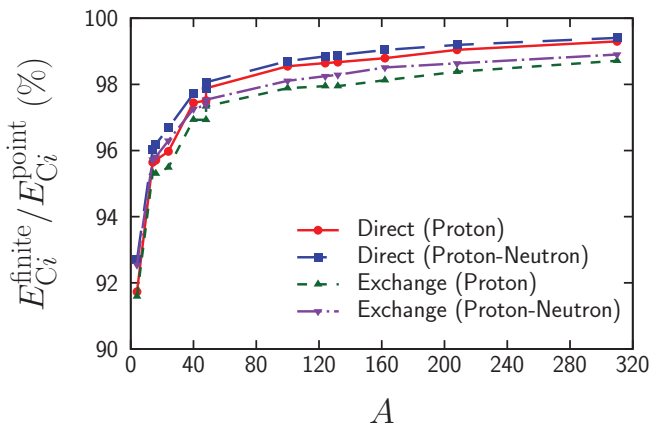


FIG. 1. Ratios of the Coulomb direct and exchange energies calculated with finite-size effects to those without the finite-size effects,  $E_{Ci}^{\text{finite}}/E_{Ci}^{\text{point}}$  ( $i = d, x$ ), shown as functions of the mass number  $A$ . The ratios for the Coulomb direct and exchange terms only with the proton finite-size effect are shown by the red solid and green dashed lines, respectively. Those with both the proton and neutron finite-size effects are shown by the blue long-dashed and purple dot-dashed lines, respectively.

the point-nucleon approximation, i.e.,  $E_{Cd}^{\text{point}}$  and  $E_{Cx}^{\text{point}}$ , are used. The proton finite-size effect and vacuum polarization are defined as the differences of the two total energies, i.e.,  $E_{\text{tot}}^{p\text{-finite}} - E_{\text{tot}}^{\text{point}}$  and  $E_{\text{tot}}^{\text{vacuum}} - E_{\text{tot}}^{pn\text{-finite}}$  where  $E_{\text{tot}}^{\text{vacuum}}$  is the total energy calculated with the all finite-size effects and vacuum polarization but without the EM spin-orbit interaction. All the energies used here are calculated with the LDA Coulomb functional. These energies are fit to

$$E = aZ^b, \quad (48)$$

where as the neutron finite-size effect defined in term of  $E_{\text{tot}}^{pn\text{-finite}} - E_{\text{tot}}^{p\text{-finite}}$  is fit to

$$E = aN^b. \quad (49)$$

These coefficients  $a$  and  $b$  are shown in Table III.

At first, the values of  $a$  and  $b$  are almost compatible with the simple estimation, performed in Sec. III. Also, as discussed above, the proton finite-size effect is one order of magnitude smaller than the exchange energy, and the neutron finite-size effect and the vacuum polarization are one more order of magnitude smaller, according to the values of  $a$  in Table III. Since the value of  $b$  for the vacuum polarization is larger than that for the neutron finite-size effect, the contribution of the vacuum polarization to the total energy is larger than that of the neutron finite-size effect in the heavy nuclei, as discussed above.

At last, the EM spin-orbit interaction gives different effects for the total energy in different nuclei. As expected, in the spin-saturated nuclei, such as  $^4\text{He}$ ,  $^{16}\text{O}$ , and  $^{40}\text{Ca}$ , the EM spin-orbit interaction contributes to

the total energy by only a few keV. In contrast, in the spin-unsaturated nuclei, the absolute values of its contribution to the total energy are around 50 keV or more. For example, on the one hand, in  $^{48}\text{Ca}$  case,  $\nu 1f_{7/2}$  orbital for neutrons is fully occupied, while its spin-orbit partner  $\nu 1f_{5/2}$  orbital is completely unoccupied. The coefficient of Eq. (29) for the  $\nu 1f_{7/2}$  orbital is negative. On the other hand, in the  $^{48}\text{Ni}$  case, the  $\pi 1f_{7/2}$  orbital for protons is fully occupied, while its spin-orbit partner  $\pi 1f_{5/2}$  orbital is completely unoccupied. The coefficient of Eq. (29) for  $\pi 1f_{7/2}$  orbital is positive. Therefore, the contribution of the EM spin-orbit interaction to the total energies for  $^{48}\text{Ca}$  and  $^{48}\text{Ni}$  should be opposite, because the corresponding contribution to the  $^{40}\text{Ca}$  core is almost zero. Indeed, as shown in Table II, its contributions for  $^{48}\text{Ca}$  and  $^{48}\text{Ni}$  are 139 keV and  $-206$  keV, respectively. The absolute value itself reflects the structure of the single-particle wave functions, in contrast with the other contributions which have just monotonic  $Z$  or  $N$  dependence.

All these corrections also change the order of some single-particle levels, as well as the total energy, for example,  $3s_{1/2}$  and  $1h_{11/2}$  for protons and  $1i_{13/2}$  and  $3p_{1/2}$  for neutrons in  $^{208}\text{Pb}$ . These effects may become even more significant in nuclei with stronger Coulomb interaction, such as the proton-rich and the superheavy nuclei.

The corrections to the Coulomb interaction are compared with the ISB energies. In light nuclei, such as the  $^{16}\text{O}$  case, the ISB terms of the nuclear force contribute to the total energy more significantly than the corrections to the EM interaction. However, in heavy nuclei, such as the  $^{208}\text{Pb}$  case, the contribution of the ISB terms of the nuclear force to the total energy is comparable to the corrections to the EM interaction, especially, the proton finite-size effect and the vacuum polarization. Therefore, once the ISB terms are considered, these corrections to the EM interaction should be also considered to keep the consistency.

The charge radii for the selected nuclei are shown in Table IV. It is seen that the charge radii calculated in the LDA and those with all the corrections to the Coulomb interaction are the same at the 0.01 fm order. In contrast, the ISB terms of the nuclear interaction can affect the charge radii around 0.1 fm. The corresponding radii become smaller, except  $^{48}\text{Ni}$  and  $^{100}\text{Sn}$ .

## B. Mirror nuclei mass difference

As a test of our framework, the mirror nuclei mass difference between  $^{48}\text{Ca}$  and  $^{48}\text{Ni}$  calculated with a combination of the Coulomb LDA or all the corrections discussed above with the present self-consistent finite-size effects (shown as ‘‘All’’ in the table) and the SAMi or SAMi-ISB functional are shown in Table V. Here, in ‘‘(All)’’ and ‘‘All,’’ the results by the conventional finite-size effects and the present self-consistent finite-size effects are shown, respectively. The experimental data are given in

TABLE II. Total energies for selected doubly magic and semimagic nuclei. All the corrections to the Coulomb interaction are considered step by step, where the SAMi functional [50] is used for the nuclear EDF. The columns labeled “LDA” and “GGA” refer to the results without the finite-size effects, while those labeled as “GGA +  $p$ -fin” and “GGA +  $pn$ -fin” refer to the results with proton and proton-neutron finite-size effects. Moreover, “VP” refers the vacuum polarization, and “All” corresponds to “GGA +  $pn$ -fin + VP + EM spin-orbit”. The column labeled as “All + ISB” is calculated with all the corrections and the SAMi-ISB functional [12]. All units are in MeV.

Nuclei	LDA	GGA	GGA + $p$ -fin	GGA + $pn$ -fin	GGA + $pn$ -fin + VP	All	All + ISB
$^4\text{He}$	-27.5263	-27.6120	-27.6748	-27.6677	-27.6597	-27.6597	-29.3137
$^{14}\text{O}$	-100.7141	-100.9292	-101.5339	-101.4800	-101.3917	-101.3684	-102.6839
$^{16}\text{O}$	-130.4800	-130.6925	-131.2765	-131.2121	-131.1245	-131.1247	-134.6588
$^{24}\text{O}$	-173.0167	-173.2203	-173.7450	-173.6534	-173.5690	-173.5204	-173.5347
$^{40}\text{Ca}$	-347.0848	-347.4582	-349.3631	-349.1581	-348.7538	-348.7544	-353.5741
$^{48}\text{Ca}$	-415.6148	-415.9813	-417.7843	-417.5394	-417.1433	-417.0041	-417.2803
$^{48}\text{Ni}$	-352.6388	-353.1148	-356.0852	-355.8364	-355.1244	-355.3307	-349.7211
$^{100}\text{Sn}$	-811.6641	-812.3382	-817.9244	-817.3322	-815.5356	-815.5896	-808.9891
$^{124}\text{Sn}$	-1047.2633	-1047.9111	-1052.8150	-1052.1049	-1050.4031	-1050.5981	-1054.9999
$^{132}\text{Sn}$	-1103.0881	-1103.7325	-1108.4618	-1107.7192	-1106.0438	-1105.9931	-1101.0821
$^{162}\text{Sn}$	-1189.5521	-1190.1618	-1194.2258	-1193.4190	-1191.8476	-1192.1076	-1192.7669
$^{208}\text{Pb}$	-1636.6149	-1637.4850	-1645.7092	-1644.4772	-1640.7825	-1640.7246	-1633.4297
$^{310}126$	-2131.4146	-2132.5366	-2145.5436	-2143.6650	-2136.3995	-2136.3397	-2125.0085

TABLE III. Parameters  $a$  and  $b$  for Eq. (48). For the neutron finite-size effect, Eq. (49) is used instead of Eq. (48).

	$a$ (MeV)	$b$
Direct Coulomb (LDA)	0.528757	1.6692
Exchange Coulomb (LDA)	-0.390342	1.0009
Exchange Coulomb (GGA)	-0.368013	1.0103
Proton Finite Size	-0.0757012	1.0640
Neutron Finite Size	0.00706328	1.0620
Vacuum Polarization	0.00354808	1.5765

TABLE IV. Charge radii for the selected nuclei. All units are shown in fm.

Nuclei	LDA	All	All + ISB
$^4\text{He}$	2.087	2.087	2.069
$^{14}\text{O}$	2.772	2.769	2.747
$^{16}\text{O}$	2.771	2.768	2.758
$^{24}\text{O}$	2.829	2.827	2.788
$^{40}\text{Ca}$	3.486	3.482	3.475
$^{48}\text{Ca}$	3.527	3.523	3.497
$^{48}\text{Ni}$	3.794	3.787	3.834
$^{100}\text{Sn}$	4.509	4.504	4.511
$^{124}\text{Sn}$	4.691	4.686	4.680
$^{132}\text{Sn}$	4.744	4.740	4.731
$^{162}\text{Sn}$	4.979	4.976	4.965
$^{208}\text{Pb}$	5.519	5.514	5.504
$^{310}126$	6.336	6.331	6.321

AME2016 [51].

At the beginning of this section, we discuss that the refitting of the functional is not needed unless the results are compared with the experimental data. Nevertheless, we can compare the calculation results with the experimental data in the mirror nuclei mass difference, since the

TABLE V. Mirror nuclei mass difference between  $^{48}\text{Ca}$  and  $^{48}\text{Ni}$  calculated with the combination of the Coulomb LDA or all the corrections to the Coulomb interaction (All) and the SAMi or SAMi-ISB functional. Here, “(All)” and “All” show the results by the conventional finite-size effects and the present self-consistent finite-size effects, respectively. The experimental data given in AME2016 [51] are also shown. All units are in MeV.

Functional	$^{48}\text{Ca}$	$^{48}\text{Ni}$	Difference
SAMi & LDA	-415.6148	-352.6388	62.9760
SAMi & (All)	-415.7756	-353.3874	62.3882
SAMi & All	-417.0041	-355.3307	61.6734
SAMi-ISB & LDA	-415.8529	-347.1168	68.7361
SAMi-ISB & (All)	-416.0248	-347.8291	68.1957
SAMi-ISB & All	-417.2803	-349.7211	67.5592
Exp. [51]	-416.000928	-348.72	67.28

contribution of the isospin symmetric part of the functional is basically canceled out.

It is seen that the mirror nuclei mass difference calculated with the Coulomb LDA functional and without the ISB terms of the nuclear force deviate more than 4 MeV from the experimental data. Even with the ISB terms of the nuclear force, still it deviates by more than 1 MeV although the result is improved. If all the corrections to the EM contribution are considered on top of the previous finite-size effects, the error is reduced. Nevertheless, the error is still around 900 keV. Once all the corrections with the novel self-consistent finite-size effects are considered in addition to the Coulomb interaction, the result is further improved and agrees, finally, with the experimental data within 300 keV error. We should notice that the refit of the SAMi functional may further improve the description of the mirror nuclei mass difference.

The Nolen-Schiffer anomaly is a related topic to the mirror nuclei mass difference [3–9]. The anomaly is the difference of mirror nuclei mass difference between theoretical calculation and experimental data. It is said that this difference comes from both the ISB terms of the nuclear interaction and the Coulomb interaction. In the present calculation, it is, actually, seen that the ISB terms of the nuclear force and the correction to the EM interaction reduce the anomaly.

## V. CONCLUSION AND PERSPECTIVES

In this paper, the finite-size effects of protons and neutrons as well as the vacuum polarization were considered in a self-consistent Skyrme Hartree-Fock calculation. The electromagnetic spin-orbit interaction was considered perturbatively. These contributions to the total energy and their systematic behavior were discussed.

The proton finite-size effect makes the nuclei more strongly bound, for example, for 8.2 MeV in  $^{208}\text{Pb}$ . In contrast, the neutron finite-size effect makes the nuclei less strongly bound, and its contribution is almost one order of magnitude smaller than the proton contribution. The contribution of the vacuum polarization to the total energy is also non-negligible, and makes the nuclei less strongly bound, for example, by 3.7 MeV in  $^{208}\text{Pb}$ . The contribution of the electromagnetic spin-orbit interaction to the total energy is around 50 keV.

Systematically, the contribution of the isospin symmetry-breaking terms of the nuclear force to the total energy is comparable to that of the proton finite-size effect in heavy nuclei, while the former is still more significant than the latter in light nuclei. The neutron finite-size effect and the vacuum polarization are also non-negligible. Meanwhile, the contribution of the electromagnetic spin-orbit interaction to the total energy depends on the shell structure.

The mirror nuclei mass difference between  $^{48}\text{Ca}$  and  $^{48}\text{Ni}$  was also calculated. All the corrections to the Coulomb functional with the SAMi-ISB functional cooperate to reproduce the mirror nuclei mass difference within 300 keV accuracy, which is improved from that calculated with conventional finite-size effects.

So far, the spherical symmetry is assumed and the pairing correlations are not considered. After considering these effects, the systematic study of the mirror nuclei mass difference is promising. The nuclear structure of the superheavy elements is also an interesting topic for applying the present scheme. Since the superheavy elements have larger  $Z$ , the highly accurate estimation of the Coulomb contribution to the binding energies is important.

Also, to reach a more accurate estimation of the Coulomb contribution to the binding energy, study of the Coulomb correlation energy is important, while this may have certain model dependence because it also includes the effects coming from the nuclear force.

## ACKNOWLEDGMENTS

The authors appreciate Shihang Shen, Enrico Vigezzi, and Kenichi Yoshida for stimulating discussions and valuable comments. T.N. and H.L. would like to thank the RIKEN iTHEMS program, the JSPS-NSFC Bilateral Program for Joint Research Project on Nuclear mass and life for unravelling mysteries of the  $r$  process, and the RIKEN Pioneering Project: Evolution of Matter in the Universe. TN acknowledges financial support from Computational Science Alliance, the University of Tokyo, Università degli Studi di Milano, and the JSPS Grant-in-Aid for JSPS Fellows under Grant No. 19J20543. H.L. acknowledges the JSPS Grant-in-Aid for Early-Career Scientists under Grant No. 18K13549. G.C. and X.R.-M. acknowledge funding from the European Union's Horizon 2020 research and innovation program under Grant No. 654002. The numerical calculations were performed on cluster computers at the RIKEN iTHEMS program.

### Appendix A: Isospin Symmetry Breaking Term of SAMi-ISB Functional

In the SAMi-ISB functional [52], the Skyrme-like zero-range charge-symmetry-breaking (CSB) and charge-independence-breaking (CIB) interactions are

$$v_{\text{CSB}}(\mathbf{r}_1, \mathbf{r}_2) = \frac{1}{4} (\tau_{z1} + \tau_{z2}) s_0 (1 + y_0 P_\sigma) \delta(\mathbf{r}_1 - \mathbf{r}_2), \quad (\text{A1})$$

$$v_{\text{CIB}}(\mathbf{r}_1, \mathbf{r}_2) = \frac{1}{2} \tau_{z1} \tau_{z2} u_0 (1 + z_0 P_\sigma) \delta(\mathbf{r}_1 - \mathbf{r}_2), \quad (\text{A2})$$

respectively, where  $\tau_{zi}$  is the  $z$  projection of the isospin operator for the  $i$ th nucleon, and  $P_\sigma = (1 + \boldsymbol{\sigma}_1 \cdot \boldsymbol{\sigma}_2) / 2$  is the spin projection operator. The parameters, including the errors attached to each parameter, are  $y_0 = z_0 = -1$ ,  $s_0 = -26.3(7) \text{ MeV fm}^3$ , and  $u_0 = 25.8(4) \text{ MeV fm}^3$ . For further details on this functional, please see Refs. [12, 46].

According to these interactions, the CSB and CIB Skyrme energy densities in the Hartree-Fock calculation are [12]

$$\mathcal{E}_{\text{CSB}}[\rho_p, \rho_n] = \frac{s_0(1-y_0)}{8} (\rho_n^2 - \rho_p^2), \quad (\text{A3})$$

$$\mathcal{E}_{\text{CIB}}[\rho_p, \rho_n] = \frac{u_0}{8} [(1-z_0)(\rho_n^2 + \rho_p^2) - 2(2+z_0)\rho_n\rho_p]. \quad (\text{A4})$$

Accordingly, the ISB average potentials for protons and

neutrons are

$$V_{\text{ISB}}^p(\mathbf{r}) = \frac{u_0(1-z_0) - s_0(1-y_0)}{4} \rho_p(\mathbf{r}) - \frac{u_0(2+z_0)}{4} \rho_n(\mathbf{r}), \quad (\text{A5})$$

$$V_{\text{ISB}}^n(\mathbf{r}) = \frac{u_0(1-z_0) + s_0(1-y_0)}{4} \rho_n(\mathbf{r}) - \frac{u_0(2+z_0)}{4} \rho_p(\mathbf{r}), \quad (\text{A6})$$

respectively.

Here, a simple estimation of the ISB energies is discussed. The proton and neutron distributions are assumed to be the hard sphere as in Sec. III:

$$\rho_\tau(r) = \begin{cases} \rho_0^\tau & r < R_\tau, \\ 0 & r > R_\tau, \end{cases} \quad (\text{A7})$$

where  $R_\tau$  is the radius of the proton or neutron distribution and

$$\rho_0^\tau = \frac{3N_\tau}{4\pi R_\tau^3} \quad (\text{A8})$$

is held ( $\tau = p, n$ ) with  $N_n = N$  and  $N_p = Z$ .

The CSB energy in this simple estimation reads

$$\begin{aligned} E_{\text{CSB}} &= \int \mathcal{E}_{\text{CSB}} d\mathbf{r} \\ &= \frac{s_0(1-y_0)}{8} \int [\{\rho_n(\mathbf{r})\}^2 - \{\rho_p(\mathbf{r})\}^2] d\mathbf{r} \\ &= \frac{s_0(1-y_0)}{8} \left( \frac{4\pi R_n^3}{3} (\rho_0^n)^2 - \frac{4\pi R_p^3}{3} (\rho_0^p)^2 \right) \\ &= \frac{s_0(1-y_0)}{8} \left( \frac{3N^2}{4\pi R_n^3} - \frac{3Z^2}{4\pi R_p^3} \right) \\ &= \frac{s_0(1-y_0)}{8} (N\rho_0^n - Z\rho_0^p), \end{aligned} \quad (\text{A9})$$

and the CIB energy reads

$$\begin{aligned} E_{\text{CIB}} &= \int \mathcal{E}_{\text{CIB}} d\mathbf{r} \\ &= \frac{u_0(1-z_0)}{8} \int [\{\rho_n(\mathbf{r})\}^2 + \{\rho_p(\mathbf{r})\}^2] d\mathbf{r} \\ &\quad - \frac{u_0(2+z_0)}{4} \int \rho_n(\mathbf{r}) \rho_p(\mathbf{r}) d\mathbf{r} \\ &= \frac{u_0(1-z_0)}{8} \left( \frac{4\pi R_n^3}{3} (\rho_0^n)^2 + \frac{4\pi R_p^3}{3} (\rho_0^p)^2 \right) \\ &\quad - \frac{u_0(2+z_0)}{4} \frac{4\pi R_p^3}{3} \rho_0^n \rho_0^p \\ &= \frac{u_0(1-z_0)}{8} \left( \frac{3N^2}{4\pi R_n^3} - \frac{3Z^2}{4\pi R_p^3} \right) \\ &\quad - \frac{u_0(2+z_0)}{4} \frac{3NZ}{4\pi R_n^3} \\ &= \frac{u_0}{8} [(1-z_0)(N\rho_0^n + Z\rho_0^p) - 2(2+z_0)Z\rho_0^n]. \end{aligned} \quad (\text{A10})$$

Here, the usual relationship  $R_n > R_p$  is assumed in Eq. (A10). If  $R_n < R_p$  is held, for example, in proton-rich nuclei, Eq. (A10) is rewritten as

$$E_{\text{CIB}} = \frac{u_0}{8} [(1-z_0)(N\rho_0^n + Z\rho_0^p) - 2(2+z_0)N\rho_0^p]. \quad (\text{A11})$$

If  $\rho_0^n = \rho_0^p = \rho_0/2 \simeq 0.08 \text{ fm}^{-3}$  is assumed as in Eq. (33), the CSB and CIB energies, Eqs. (A9) and (A10), are evaluated as

$$\begin{aligned} E_{\text{CSB}} &= \frac{s_0(1-y_0)}{8} (N-Z)\rho_0 \\ &\simeq -0.526(N-Z) \text{ MeV}, \end{aligned} \quad (\text{A12})$$

$$\begin{aligned} E_{\text{CIB}} &= \frac{u_0}{8} [(1-z_0)(N+Z)\rho_0 - 2(2+z_0)Z\rho_0] \\ &\simeq [0.516(N+Z) - 0.516Z] \text{ MeV} \\ &\simeq 0.516N \text{ MeV}. \end{aligned} \quad (\text{A13})$$

- 
- [1] J. C. Hardy and I. S. Towner, *Phys. Rev. C* **91**, 025501 (2015).
- [2] H. Liang, N. Van Giai, and J. Meng, *Phys. Rev. C* **79**, 064316 (2009).
- [3] K. Okamoto, *Phys. Lett.* **11**, 150 (1964).
- [4] J. A. Nolen, Jr. and J. P. Schiffer, *Annu. Rev. Nucl. Sci.* **19**, 471 (1969).
- [5] K. Saito and A. Thomas, *Phys. Lett. B* **335**, 17 (1994).
- [6] M. H. Shahnas, *Phys. Rev. C* **50**, 2346 (1994).
- [7] U. G. Meißner, A. M. Rakhimov, A. Wirzba, and U. T. Yakhshiev, *Eur. Phys. J. A* **36**, 37 (2008).
- [8] D. P. Menezes, S. S. Avancini, C. Z. Vasconcellos, and M. Razeira, *Eur. Phys. J. A* **42**, 97 (2009).
- [9] J. M. Dong, Y. H. Zhang, W. Zuo, J. Z. Gu, L. J. Wang, and Y. Sun, *Phys. Rev. C* **97**, 021301 (2018).
- [10] J. Jänecke, *Nucl. Phys.* **73**, 97 (1965).
- [11] S. Shlomo, *Rep. Prog. Phys.* **41**, 957 (1978).
- [12] X. Roca-Maza, G. Colò, and H. Sagawa, *Phys. Rev. Lett.* **120**, 202501 (2018).
- [13] P. Bączyk, J. Dobaczewski, M. Konieczka, W. Satuła, T. Nakatsukasa, and K. Sato, *Phys. Lett. B* **778**, 178 (2018).
- [14] P. Bączyk, W. Satuła, J. Dobaczewski, and M. Konieczka, *J. Phys. G* **46**, 03LT01 (2019).
- [15] P. Hohenberg and W. Kohn, *Phys. Rev.* **136**, B864 (1964).
- [16] W. Kohn and L. J. Sham, *Phys. Rev.* **140**, A1133 (1965).
- [17] M. Bender, P.-H. Heenen, and P.-G. Reinhard, *Rev. Mod. Phys.* **75**, 121 (2003).
- [18] T. Nakatsukasa, K. Matsuyanagi, M. Matsuo, and K. Yabana, *Rev. Mod. Phys.* **88**, 045004 (2016).
- [19] X. Roca-Maza and N. Paar, *Prog. Part. Nucl. Phys.* **101**, 96 (2018).
- [20] D. Vautherin and D. M. Brink, *Phys. Rev. C* **5**, 626 (1972).
- [21] J. Berger, M. Girod, and D. Gogny, *Comput. Phys. Commun.* **63**, 365 (1991).
- [22] J. Meng, H. Toki, S. Zhou, S. Zhang, W. Long, and L. Geng, *Prog. Part. Nucl. Phys.* **57**, 470 (2006).
- [23] H. Liang, J. Meng, and S.-G. Zhou, *Phys. Rep.* **570**, 1 (2015).
- [24] P. A. M. Dirac, *Proc. Camb. Phil. Soc.* **26**, 376 (1930).
- [25] J. C. Slater, *Phys. Rev.* **81**, 385 (1951).
- [26] H.-Q. Gu, H. Liang, W. H. Long, N. Van Giai, and J. Meng, *Phys. Rev. C* **87**, 041301 (2013).
- [27] N. Van Giai, H. Liang, H.-Q. Gu, W. Long, and J. Meng, *Phys. Scr.* **89**, 054008 (2014).
- [28] X. Roca-Maza, L.-G. Cao, G. Colò, and H. Sagawa, *Phys. Rev. C* **94**, 044313 (2016).
- [29] T. Naito, R. Akashi, and H. Liang, *Phys. Rev. C* **97**, 044319 (2018).
- [30] T. Naito, X. Roca-Maza, G. Colò, and H. Liang, *Phys. Rev. C* **99**, 024309 (2019).
- [31] B. Alex Brown, *Phys. Rev. C* **58**, 220 (1998).
- [32] N. Chamel, S. Goriely, and J. M. Pearson, *Phys. Rev. C* **80**, 065804 (2009).
- [33] Z. M. Niu, Q. Liu, Y. F. Niu, W. H. Long, and J. Y. Guo, *Phys. Rev. C* **87**, 037301 (2013).
- [34] J.M. Dong, X.L. Shang, W. Zuo, Y.F. Niu, and Y. Sun, *Nucl. Phys. A* **983**, 133 (2019).
- [35] A. Bulgac and V. R. Shaginyan, *Nucl. Phys. A* **601**, 103 (1996).
- [36] N. Auerbach, J. Hüfner, A. K. Kerman, and C. M. Shakin, *Rev. Mod. Phys.* **44**, 48 (1972).
- [37] J. P. Perdew, K. Burke, and M. Ernzerhof, *Phys. Rev. Lett.* **77**, 3865 (1996).
- [38] L. Ray, *Phys. Rev. C* **19**, 1855 (1979).
- [39] J. Friedrich and T. Walcher, *Eur. Phys. J. A* **17**, 607 (2003).
- [40] E. Engel and R. M. Dreizler, *Density Functional Theory—An Advanced Course*, Theoretical and Mathematical Physics (Springer-Verlag, Berlin, Heidelberg, 2011).
- [41] N. Auerbach, *Phys. Lett. B* **282**, 263 (1992).
- [42] S. Weinberg, *The Quantum Theory of Fields* (Cambridge University Press, 1995).
- [43] E. A. Uehling, *Phys. Rev.* **48**, 55 (1935).
- [44] E. Tiesinga, P. J. Mohr, D. B. Newell, and B. N. Taylor, “The 2018 CODATA Recommended Values of the Fundamental Physical Constants,” (2019).
- [45] L. Wayne Fullerton and G. A. Rinker, *Phys. Rev. A* **13**, 1283 (1976).
- [46] X. Roca-Maza, G. Colò, and H. Sagawa, *EPJ Web Conf.* **194**, 01002 (2018).
- [47] W. Greiner, *Quantum Mechanics—Special Chapters* (Springer-Verlag, Berlin, Heidelberg, 1998).
- [48] E. Chabanat, P. Bonche, P. Haensel, J. Meyer, and R. Schaeffer, *Nucl. Phys. A* **627**, 710 (1997).
- [49] G. Colò, L. Cao, N. Van Giai, and L. Capelli, *Comput. Phys. Commun.* **184**, 142 (2013).
- [50] X. Roca-Maza, G. Colò, and H. Sagawa, *Phys. Rev. C* **86**, 031306 (2012).
- [51] W. Huang, G. Audi, M. Wang, F. G. Kondev, S. Naimi, and X. Xu, *Chin. Phys. C* **41**, 030002 (2017).
- [52] H. Sagawa, N. Van Giai, and T. Suzuki, *Phys. Lett. B* **353**, 7 (1995).